Available online at www.sciencedirect.com
ScienceDirect
Comput. Methods Appl. Mech. Engrg. 365 (2020) 112959
Computer methods in applied mechanics and engineering
www.elsevier.com/locate/cma

Bayesian inversion for electrical-impedance tomography in medical imaging using the nonlinear Poisson–Boltzmann equation

Leila Taghizadeh[a,*], Ahmad Karimi[a], Benjamin Stadlbauer[a], Wolfgang J. Weninger[c], Eugenijus Kaniusas[d], Clemens Heitzinger[a,b]

[a] *Institute for Analysis and Scientific Computing, Vienna University of Technology (TU Wien), Wiedner Hauptstraße 8–10, 1040 Vienna, Austria*
[b] *School of Mathematical and Statistical Sciences, Arizona State University, Tempe, AZ 85287, USA*
[c] *Division of Anatomy, MIC, Medical University of Vienna & CMI, Währingerstraße 13, 1090 Vienna, Austria*
[d] *Institute of Electrodynamics, Microwave and Circuit Engineering, Vienna University of Technology (TU Wien), Gußhausstraße 27/354, 1040 Vienna, Austria*

Received 29 April 2019; received in revised form 22 January 2020; accepted 20 February 2020
Available online xxxx

Abstract

We develop an electrical-impedance tomography (EIT) inverse model problem in an infinite-dimensional setting by introducing a nonlinear elliptic PDE as a new EIT forward model. The new model completes the standard linear model by taking the transport of ionic charge into account, which was ignored in the standard equation. We propose Bayesian inversion methods to extract electrical properties of inhomogeneities in the main body, which is essential in medicine to screen the interior body and detect tumors or determine body composition. We also prove well-definedness of the posterior measure and well-posedness of the Bayesian inversion for the presented nonlinear model. The new model is able to distinguish between liquid and tissues and the state-of-the-art delayed-rejection adaptive-Metropolis (DRAM) algorithm is capable of analyzing the statistical variability in the measured data in various EIT experimental designs. This leads to design a reliable device with higher resolution images which is crucial in medicine for diagnostic purposes. We first test the validation of the presented nonlinear model and the proposed inverse method using synthetic data on a simple square computational domain with an inclusion. Then we establish the new model and robustness of the proposed inversion method in solving the ill-posed and nonlinear EIT inverse problem by presenting numerical results of the corresponding forward and inverse problems on a real-world application in medicine and healthcare. The results include the extraction of electrical properties of human leg tissues using measurement data.

Keywords: Electrical impedance tomography; Uncertainty quantification; Medical imaging; Inverse modeling; Bayesian inversion; Data science

* Corresponding author.
E-mail addresses: leila.taghizadeh@tuwien.ac.at (L. Taghizadeh), ahmad.karimi@tuwien.ac.at (A. Karimi), benjamin.stadlbauer@tuwien.ac.at (B. Stadlbauer), wolfgang.weninger@meduniwien.ac.at (W.J. Weninger), eugenijus.kaniusas@tuwien.ac.at (E. Kaniusas), clemens.heitzinger@tuwien.ac.at (C. Heitzinger).

https://doi.org/10.1016/j.cma.2020.112959

1. Introduction

Tomography is one of the most important techniques in imaging and could be used in medical monitoring such as monitoring for internal bleeding, screening for breast cancer, detection of pulmonary emboli and blood clots in lungs, provided that the corresponding inverse problems can be reliably solved. Imaging the internal organs to diagnose diseases is one of the most important aspects of modern medicine. Many medical problems could be easily diagnosed by information about the distribution of electrical properties inside the body. Although tomography has originally been used solely in medical imaging, in its general sense it has now become much more diverse and is used in a wide range of fields including industrial and geophysical applications. It is used in industrial-process tomography to control industrial processes such as curing and cooking. Geophysical surveying is another application of the technique which is used for determining the location of mineral and oil deposits, leakage detection in pipes, etc. Furthermore, atmospheric and forensic imaging, archeology, and land-mine detection are other fields where tomography imaging is used.

Since modern medicine relies on imaging methods, the mathematics of tomography have become one of the most important applications of mathematics in the areas of healthcare, medicine, and life sciences in general. In soft-field tomographic techniques, a sensing field is applied to an object and the responses to this field are measured. Processing of these responses allows reconstruction of the distributions of physical properties inside the object, if the nonlinear inverse problem can be solved. For instance, electrical-impedance tomography (EIT) [1] in medicine, electrical-resistance tomography (ERT) [2] in geophysical applications, and electrical-capacitance tomography (ECT) [3] in industrial process monitoring are soft-field tomography techniques. The nature of soft-field tomography techniques is much more complex than the nature of hard-field ones and requires considerably more computational analysis and algorithms to reconstruct the image.

Tomography is defined as measuring the propagation of energy or particle motion in order to reconstruct information about the interior of a system. Usually this information is a reconstruction of electrical and geometrical properties of the system such as conductivity, charge, and size. Hence parameter reconstruction in soft-field tomography is based on an inverse problem, where a forward model is fitted to the data. In medical applications, computed tomography (CT) and EIT are the two main methods used in imaging and reconstruction. The CT reconstruction problem is a linear problem since X-rays propagate in straight lines through the object and their absorption at any point inside the object is independent of the absorption at any other point. Therefore, the attenuation is measured along each collimated beam direction, which is a linear problem and leads to sparse and well-conditioned sensitivity matrices (Radon transforms). In this method, the device is usually very complicated and provides very good resolution. Electrical-impedance tomography is an imaging technique for detecting (and imaging) internal properties such as the conductivity distribution inside an object by means of measuring the electrical properties at exterior electrodes. A set of contact electrodes is attached on the surface of the body and prescribed electric potentials are applied to the body through the electrodes. The corresponding electrical currents needed to maintain these potentials are measured on these electrodes. The EIT reconstruction is a nonlinear and ill-posed inversion problem. It is nonlinear since as the field is modified inside the body, the potential measured at the boundary of the domain is a nonlinear function of the distribution of the electrical properties through the body. Furthermore, this problem is ill-posed, since large changes in the interior can correspond to very small changes in the measured data [4]. The resulting resolution of EIT is lower than the one of CT, but practical advantages such as simple, cheap, portable, and radiation free devices have put this method into the center of attention in recent years.

The idea behind the EIT technology is not new as the idea of electrical-resistive tomography was proposed in 1978, independently by Henderson and Webster for medical imaging, and by Lytle and Dines for geophysical imaging [5]. Since that time, computational power has increased and more efficient inverse algorithms have been proposed. Hence, due to this fact and as it includes crucial applications, looking at the idea again and applying modern and powerful inverse algorithms such as Bayesian-estimation methods to analyze the results is of great importance.

There are fundamental differences between classical and Bayesian inverse modeling. The first difference is in the nature of the solution; the solution of Bayesian estimation is a probability distribution of the model parameter, which is a random variable. Hence a confidence interval for each of the quantities of interest can be found, which is crucial in applications such as in medicine. The other difference is using prior knowledge in the Bayesian approach to update the current information about the parameters of interest. The connection between the two level of knowledge is made by means of Bayes' Theorem. In Bayesian estimation techniques, Markov-chain Monte-Carlo (MCMC)

methods [6–9] and adaptive MCMC algorithms [10–12] are used to deal with inverse problems in order to circumvent the need to calculate high-dimensional integrals (appearing in Bayes' Theorem). Moreover they sample the space efficiently and completely search the space. Bayesian approaches to the EIT inverse problem have previously been studied, for example in [13–16]. Bayesian inference for inverse problems, especially in infinite dimensions is a new approach, which has been applied to linear (e.g. [17]) and recently nonlinear problems (e.g. [18,19]).

In this work, we focus on electrical-impedance tomography as a soft-field tomography technique and one of the main imaging techniques applied in medicine. We present and solve an elliptic partial differential equation, namely a nonlinear Poisson–Boltzmann equation as the EIT model to find the electrical currents flowing in and out of the electrodes in a bioimpedance tomography device. This is the first paper that uses this nonlinear model for the EIT problem in order to take the free charges present in the problem into account and gives the related Bayesian formulation in an infinite-dimensional setting in order to solve the corresponding inverse problem. We solve the EIT forward problem by means of the first order Galerkin finite-element (GFE) approximation and a mesh generated by the GMSH package [20]. For solving the corresponding inverse problem, an adaptive MCMC method, namely the delayed-rejection adaptive-Metropolis (DRAM) algorithm is proposed, which is based on the combination of two powerful ideas: adaptive Metropolis (AM) [21,22] and delayed-rejection (DR) [23,24], which are used as global and local adaptive algorithms to modify the MCMC method. All algorithms for Bayesian inversion in this work have been implemented in the Julia programming language [25,26]. Numerical results using the state-of-the-art GFE and the adaptive MCMC illustrate accurate extraction of the quantities of interest in the EIT inverse problem. We evaluate the presented nonlinear model and the proposed inversion method first on a simple geometry as the computational domain and using synthetic data. Then we apply it on a real-world application in medicine to estimation of muscle conductivity in a cross-section of leg using measurement data. As a result, the confidence interval of unknown quantity using the proposed forward model and the inversion method is calculated. This application is important since usually muscle absorbs water which decreases its conductivity. The presented model is capable of distinguishing water and muscle due to the nonlinear term and hence detecting muscle tissues more accurately and producing high resolution images, which is important for precisely determining the body composition. On the other hand, the accuracy of results and higher resolution of reconstructed images are crucial in medicine for diagnostic purposes.

We also present Bayesian inversion for the presented nonlinear elliptic PDE model for EIT in the measure-theoretic framework and prove that the posterior measure is Lipschitz continuous in the data to conclude well-definedness and well-posedness of the resulting posterior measures obtained by the Bayesian technique.

The paper is organized as follows: In Section 2, the new nonlinear model as the EIT forward problem is presented. Section 3 is devoted to the EIT inverse problem. In this section, first Bayesian estimation in the measure theoretic framework is formulated and then well-definedness and well-posedness of Bayesian inversion for the new EIT model are proved. In Section 4, numerical experiments of the presented model and the proposed inversion method on a test problem are illustrated. The examination of the methodology on a real-world application using measurement data is presented in Section 5. These results show the capability of the Bayesian approach to identify the unknown quantities in the EIT inverse problem corresponding to the new model and support our theoretical findings. Finally, conclusions are drawn in Section 6.

2. The EIT nonlinear model

The presence of liquids such as blood in human body is unavoidable. Therefore, in order to design an accurate and reliable EIT sensor, we need to take them into account in the computational model. We extend the standard model to the nonlinear one by simulating the transport of free charges in the background medium, which was ignored in the standard model. The new model can distinguish between the liquid and the other materials and therefore the inverse problem associated with this model results in more accurate reconstructed images with higher resolution. In this section, first we briefly review the derivation of the standard linear EIT problem, and then present the nonlinear model. We give the required assumptions for the existence and uniqueness of solution to the new PDE model as well.

We assume a square domain as a cross-section of the main object under consideration containing an inclusion consisting of a different material than the background medium and with eight electrodes which are equidistantly attached to the surface of the main body. The device with this configuration will be used as the computational domain

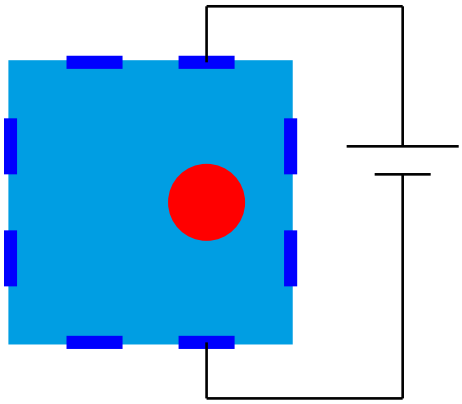

Fig. 1. Schematic diagram of a cross-section of an EIT device with eight electrodes attached to the boundary of the main object including one inclusion used for the test problem.

for the test problem later. In Fig. 1, a schematic diagram of the device with one of the measurement patterns is shown. In this pattern, a potential is applied between two electrodes, and the resulting electrical current is measured at the rest of the electrodes. The forward problem is to find the electrostatic potential in the physical domain and then to calculate the electrical current flowing through the electrodes. Assume that $D \subset \mathbb{R}^n, n \in \{2, 3\}$, is a closed and bounded domain with a smooth boundary ∂D. Using the quasi-static approximation, the electrical field E can be represented in terms of a scalar potential u by

$$E(x) = -\nabla u(x), \tag{1}$$

where $x \in D$. For simplicity we assume direct current or sufficiently low-frequency current such that the magnetic field can be neglected. In the case of direct currents, in which the applied voltage is independent of time, the derivation is simple. The electric potential u results in the current density J, which satisfies the continuum Ohm's law $J = -A\nabla u$, where A is the admittivity [27]. In the absence of current sources in the interior of the body, the continuum version of Kirchoff's law $\nabla \cdot J = 0$ results in the elliptic PDE

$$\nabla \cdot (A\nabla u) = 0.$$

In the case of alternating currents, we consider the time-harmonic Maxwell's equations at a fixed angular frequency ω, and it is assumed that the transient components of all fields are negligible [27]. Ignoring magnetic effects, we substitute Eq. (1) into the time-harmonic Maxwell's equations, while assuming no internal current source in EIT problems, and take the divergence on the both sides to obtain the (complex-valued) linear model

$$\nabla \cdot (A\nabla u) = 0, \tag{2}$$

where

$$A(x, \omega) \coloneqq \sigma(x, \omega) + i\omega\epsilon(x, \omega) \tag{3}$$

is the admittivity, and σ and ϵ are the electric conductivity and permittivity, respectively. Also, ω is the frequency of the electrical current. Since we restrict the present discussion to static fields, i.e., $\omega \to 0+$, the admittivity is real and coincides with the static conductivity, i.e. $A = \sigma(x)$, which we use here. Moreover, the impedivity $\rho = 1/A$ is just the resistivity of the body [28]. The linear model (2) is widely used for modeling EIT; the Electrical Impedance Tomography and Diffuse Optical Tomography Reconstruction Software EIDORS [29] (http://eidors.org) is based on this model equation.

To find the boundary conditions, we assume that there are L contact electrodes e_ℓ, which are attached to the surface of the body, i.e.,

$$e_\ell \subset \partial D, \quad 1 \le \ell \le L, \tag{4}$$

such that $\overline{e}_\ell \cap \overline{e}_k = \emptyset$ for $\ell \neq k$. We assume that the electrodes conduct perfectly, and thus the tangential electrical field vanishes along the electrodes. Then possible boundary conditions on the electrodes are the Dirichlet boundary

conditions

$$u(x) = U_\ell, \quad x \in e_\ell, \quad 1 \le \ell \le L. \tag{5}$$

We also assume that no current flows in and out of the body between the electrodes, which leads to zero Neumann boundary condition

$$\frac{\partial u(x)}{\partial \mathbf{n}} = 0, \quad x \in \partial D \backslash \bigcup_{\ell=1}^{L} e_\ell. \tag{6}$$

Assuming that the energies of all ions in the electric field are distributed according to a Boltzmann distribution, we define the charge density of free charges in the system by

$$f_{\text{free}} := \eta(\exp(-\beta u) - \exp(\beta u)) = -2\eta \sinh(\beta u),$$

where η is the ion accessibility function. The constant β is defined as $\beta := 1/U_T$, where U_T is the thermal voltage at room temperature and it is defined by $U_T := k_B T/q$ in terms of the Boltzmann constant k_B and the temperature T, and $q > 0$ the elementary charge. Here we assume that the charge of single positive and negative charge carriers are the same. In the definition of charge density of free charges, the exponential terms stem from the Boltzmann distributions for two species of ions, which lead to sinh in the model.

Adding charge density of free charges f_{free} to the fixed charges f_{fixed} (for simplicity we denote it by f in the equation), we arrive at the nonlinear Poisson–Boltzmann equation

$$-\nabla \cdot (A(x)\nabla u(x)) = f(x) - 2\eta(x)\sinh(\beta u(x))$$

as the extended model for the EIT problem. Therefore, the new forward problem describing EIT is to find the potential u in the main object D, given the conductivity A, the voltage pattern $U = [U_1, \ldots, U_L]^T$, the ion accessibility function η, and the concentration f of fixed charges, that solves the (real-valued) nonlinear elliptic PDE

$$-\nabla \cdot (A(x)\nabla u(x)) + 2\eta(x)\sinh(\beta u(x)) = f(x) \qquad \forall x \in D, \tag{7a}$$

$$u(x) = U_\ell \qquad \forall x \in e_\ell, \tag{7b}$$

$$\frac{\partial u(x)}{\partial \mathbf{n}} = 0 \qquad \forall x \in \partial D \backslash \bigcup_{\ell=1}^{L} e_\ell. \tag{7c}$$

As mentioned before, in every measurement pattern a potential is applied to the electrodes and the resulting electrical current on the rest of the electrodes is measured. The electrical current flowing through the electrodes in the EIT problem [4] is calculated by

$$I_\ell = \int_{e_\ell} A \frac{\partial u(x)}{\partial \mathbf{n}} ds, \qquad \ell = 1, 2, \ldots, L. \tag{8}$$

The nonlinear Poisson–Boltzmann equation (7) has a unique solution and a pointwise estimate for the solution of the equation has been presented in [30]. The required assumptions for existence of a unique solution are listed below:

Assumptions 1. The conductivity $A\colon D \to \mathbb{R}^{2\times 2}$ and the voltage simulation pattern $\{U_\ell\}_{\ell=1}^{L} \in \mathbb{R}^L$ satisfy the following assumptions:

1. The coefficient $A\colon D \to \mathbb{R}^{2\times 2}$ is a piecewise constant-valued matrix, which is uniformly elliptic and satisfies
$$A \in L^\infty(D; \mathbb{R}^{2\times 2}), \quad \operatorname*{ess\,inf}_{x\in D} A(x) = A^- > 0 \tag{9}$$
and contains the conductivity of the inclusion or background medium, as the two materials are different in their physical properties.
2. The voltage applied to the ℓ-th electrode is chosen such that $\sum_{\ell=1}^{L} U_\ell = 0$.

3. The EIT inverse problem associated with the nonlinear forward model

The EIT inverse problem is to reconstruct the electrical and physical properties of the body interior, given the electrical current measurements on its surface. Bayesian inferences [31–34] applied to the EIT inverse problem corresponding to the standard linear forward model (2) has previously been studied. This inversion method for nonlinear inverse problems in infinite dimensions is a new approach. In this work, we propose Bayesian estimation methods to the EIT inverse problem corresponding to the presented nonlinear forward model (7), as this inversion technique was capable of dealing with ill-posedness and nonlinearity of problems in many applications [35–37]. Here we will also show this claim about the EIT inverse problem by numerical results on a test problem and then on a real-world application in medicine. Our goal in this section is to show well-definedness of the posterior measure obtained by the Bayesian techniques as well as well-posedness of the Bayesian inversion for the EIT inverse model associated with the nonlinear forward model presented in the previous section. To this end, we first present the mathematical formulation of the Bayesian analysis in a measure-theoretic framework and in the infinite-dimensional setting. Then, our main theoretical results are stated and proved in Proposition 1. These results include boundedness and Lipschitz continuity of the solution of the physical model by functions of the parameters, which lead to well-definedness and well-posedness of the applied Bayesian estimation method for the prescribed model in the EIT technology.

3.1. Bayesian analysis in a measure-theoretic framework

In Bayesian estimation technique, solution of the inverse problem is the posterior density that best reflects the distribution of the parameter based on the observations. As the observations or measurements are subject to noise and the observational noise, i.e., the error e due to modeling and measurement, is unbiased and iid, it can be represented by random variables as

$$M = G(Q) + e, \tag{10}$$

where e is a mean-zero random variable and M is a given random variable representing observed data or measurements, for which we have a model $G(Q)$ (observation operator) dependent on a random variable Q with realizations $q = Q(\omega)$ representing parameters to be estimated [31].

To describe the Bayesian approach on function spaces, we formulate Bayes' Theorem in a measure-theoretic framework, which is suitable for problems on infinite-dimensional spaces. To this end, assume that $(X, \|\cdot\|_X)$ (infinite-dimensional) and $(Y, \|\cdot\|_Y)$ (possibly infinite-dimensional) are separable Banach spaces and that $G\colon X \to Y$ is the observation operator. Therefore, let $q \in X$ be a random variable distributed according to measure μ_0 on X, in which our prior beliefs about the unknown parameter q are described. We assume the distribution of the measurement error e (data likelihood) is defined by

$$\pi(y|q) := \pi(y - G(q)) \tag{11}$$

to calculate the posterior probability measure μ^y for $q \in X$ given $y \in Y$, which leads to

$$\pi(q|y) = \frac{\pi_0(q)\pi(y - G(q))}{\int_{\mathbb{R}^p} \pi_0(q)\pi(y - G(q))\mathrm{d}q} \tag{12}$$

using Bayes' formula, where π_0 and π are the prior and posterior density functions and correspond to the probability measures μ_0 and μ^y, respectively. Thus we have

$$\pi(q|y) \propto \pi_0(q)\pi(y - G(q)) \tag{13}$$

with a constant of proportionality depending only on y.

As in infinite-dimensional spaces there is no density with respect to the Lebesgue measure, Bayes' rule should be interpreted as providing the Radon–Nikodym derivative between the posterior measure $\mu^y(\mathrm{d}q) = P(\mathrm{d}q|y)$ (with density $\pi(q|y)$) and the prior measure $\mu_0(\mathrm{d}q) = P(\mathrm{d}q)$ (with density π_0), yielding

$$\frac{\mathrm{d}\mu^y}{\mathrm{d}\mu_0}(q) \propto \pi(y - G(q)). \tag{14}$$

Without loss of generality, we can view the right-hand side as the exponential of the negative of $\Phi(q, y)$, where $\Phi\colon X \times Y \to \mathbb{R}$ is called a potential. Hence Eq. (14) can be rewritten as

$$\frac{\mathrm{d}\mu^y}{\mathrm{d}\mu_0}(q) \propto \exp(-\Phi(q, y)), \tag{15}$$

since the density π is nonnegative [18]. Furthermore, the posterior measure μ^y in some PDE inverse problems can be formulated as

$$\frac{\mathrm{d}\mu^y}{\mathrm{d}\mu_0}(q) = \frac{1}{C(y)} \exp(-\Phi(q, y)), \tag{16}$$

where $C(y)$ is a normalization constant and chosen such that μ^y is a probability measure, i.e.,

$$C(y) := \int_X \exp(-\Phi(q, y))\mathrm{d}\mu_0(q). \tag{17}$$

Furthermore, we assume that $\mu_0(X) = 1$ holds for the infinite-dimensional separable Banach space X.

The goal is to show that the posterior measure μ^y of the form (16) is well-defined and that the problem is well-posed with respect to its dependence on the data. To this end, the function $\Phi\colon X \times Y \to \mathbb{R}$ should have essential properties, namely lower and upper bounds and the Lipschitz property in q and y. As this function is defined in terms of the function $G\colon X \to \mathbb{R}^m$, it is sufficient to prove the following properties of the function G corresponding to the inverse problem of interest. This implies that $\Phi\colon X \times \mathbb{R}^m \to \mathbb{R}$ satisfies Assumption 2.6 in [18] with $(Y, \|\cdot\|_Y) = (\mathbb{R}^m, |\cdot|)$.

Assumptions 2. The function $G\colon X \to \mathbb{R}^m$ has the following properties.

1. For every $\varepsilon > 0$, there exists an $M(\varepsilon) \in \mathbb{R}$ such that the inequality
$$|G(q)| \leq \exp(\varepsilon\|q\|_X^2 + M(\varepsilon)) \tag{18}$$
holds for all $q \in X$.
2. For every $r > 0$, there exists a $K(r) > 0$ such that the inequality
$$|G(q_1) - G(q_2)| \leq K(r)\|q_1 - q_2\|_X \tag{19}$$
holds for all $q_1, q_2 \in X$ with $\max(\|q_1\|_X, \|q_2\|_X) < r$.

To prove the well-definedness of the posterior measure and well-posedness of the EIT Bayesian inversion, we need to verify if the bounds and Lipschitz properties in Assumption 2 hold true when G is given by the solution of the (real-valued) nonlinear elliptic PDE

$$-\nabla \cdot (A(x)\nabla u(x)) + 2\eta(x)\sinh(\beta u(x)) = 0 \qquad \forall x \in D, \tag{20a}$$

$$u(x) = g \qquad \forall x \in \partial D_D, \tag{20b}$$

$$\frac{\partial u(x)}{\partial \mathbf{n}} = 0 \qquad \forall x \in \partial D_N, \tag{20c}$$

where ∂D_D and ∂D_N denote the Dirichlet and Neumann boundaries. In (20), the solution u can be the real or the imaginary part of the solution of the complex-valued model (2)–(3), i.e., either $\Re(u)$ or $\Im(u)$. Here, for the sake of simplicity we denote the solution of the real-valued model (20) by u as well. We present the results in Section 3.2 as a proposition.

The nonlinear Poisson–Boltzmann equation (20) has a unique solution. Moreover a pointwise estimate for the solution of the equation has been presented in [30], which will be used later.

3.2. Main theoretical results

Here, the main results including the well-definedness of the posterior measure and well-posedness of the EIT Bayesian inversion for the new model (20) are presented. To this end, the validity of Assumption 2 should be verified in the sense that a parameter dependent bound for the solution of the nonlinear model equation must be found and the Lipschitz property of the solution must hold true as well. We have collected our theoretical findings for the new model in Proposition 1. For the linear model a similar bound and the Lipschitz property has been already proved in [38].

Proposition 1. *Suppose the real-valued nonlinear elliptic equation (20) holds in the bounded domain $D \subset \mathbb{R}^n$, $n \in \{2, 3\}$, with a smooth boundary ∂D and $A := e^q =: \eta$, where $q \in L^\infty(D)$. Then the estimate*

$$\|u\|_{H^1} \leq H e^{2\|q\|_{L^\infty}} \tag{21}$$

holds for all $q \in L^\infty(D)$, and the estimate

$$\|u_1 - u_2\|_{H^1} \leq S e^{4\max(\|q_1\|_{L^\infty(D)}, \|q_2\|_{L^\infty(D)})} \|q_1 - q_2\|_{L^\infty(D)} \tag{22}$$

holds for all $q_1, q_2 \in L^\infty(D)$, where $H = H(\|\nabla \overline{g}\|_{L^2(D)})$ and $S = S(\|\nabla \overline{g}\|_{L^2(D)})$ are functions and $\overline{g} \in L^2(D)$ is the Dirichlet lift of g.

Proof. We substitute $v := u - \overline{g}$ in (20), where $\overline{g}$ is the Dirichlet lift of g. It is defined by

$$\overline{g} := \begin{cases} g & \text{on } \partial D, \\ \text{arbitrary} & \text{in } D \end{cases} \tag{23}$$

such that $\overline{g} \in L^2(D)$.

In order to find estimates (21) and (22), we take the inner product with any $v \in H_0^1(D)$, which leads to

$$I := \left| \int A \nabla v \cdot \nabla v \right| = \left| - \int A \nabla \overline{g} \cdot \nabla v - \int 2\eta \sinh(\beta(\overline{g} + v)) v \right|,$$

where $A = e^q$. Using $\eta = e^q$ and $\sinh(\beta(\overline{g} + v)) = (e^{\beta(\overline{g}+v)} - e^{-\beta(\overline{g}+v)})/2$ as well as the triangle inequality, we find

$$e^{-\|q\|_{L^\infty}} \|\nabla v\|_{L^2}^2 \leq I \leq \left| \int e^q \nabla \overline{g} \cdot \nabla v \right| + \left| \int e^q e^{\beta(\overline{g}+v)} v \right| + \left| \int e^q e^{-\beta(\overline{g}+v)} v \right|.$$

Using the Cauchy–Schwarz and Poincaré inequalities and $\kappa \leq u = \overline{g} + v \leq \lambda$, which is a pointwise estimate [30] for the solution of the Poisson–Boltzmann equation, we can write

$$e^{-\|q\|_{L^\infty}} \|\nabla v\|_{L^2}^2 \leq I \leq e^{\|q\|_{L^\infty}} (\|\nabla \overline{g}\|_{L^2} + C_p e^{|\beta\lambda|} + C_p e^{|\beta\kappa|} \|\nabla v\|_{L^2}),$$

where C_p is a Poincaré constant and κ and λ are constants. Therefore, we calculate

$$\begin{aligned} \|\nabla u\|_{L^2} &\leq \|\nabla v\|_{L^2} + \|\nabla \overline{g}\|_{L^2} \\ &\leq e^{2\|q\|_{L^\infty}} (\|\nabla \overline{g}\|_{L^2} + C_p e^{|\beta\lambda|} + C_p e^{|\beta\kappa|}) + \|\nabla \overline{g}\|_{L^2} \\ &= (1 + e^{2\|q\|_{L^\infty}}) \|\nabla \overline{g}\|_{L^2} + C_p e^{2\|q\|_{L^\infty}} (e^{|\beta\lambda|} + e^{|\beta\kappa|}) \\ &\leq 2C_p e^{2\|q\|_{L^\infty}} (\|\nabla \overline{g}\|_{L^2} + e^{|\beta\lambda|} + e^{|\beta\kappa|}) \\ &= H_0 e^{2\|q\|_{L^\infty}}, \end{aligned} \tag{24}$$

where $H_0 := 2C_p(\|\nabla \overline{g}\|_{L^2} + e^{|\beta\lambda|} + e^{|\beta\kappa|})$. Using the definition of H^1-norm and inequality (24), we can write

$$\frac{1}{(1 + C_p^2)^{1/2}} \|u\|_{H^1} \leq \|\nabla u\|_{L^2} \leq H_0 e^{2\|q\|_{L^\infty}},$$

where C_p is a Poincaré constant. This leads to

$$\|u\|_{H^1} \leq H e^{2\|q\|_{L^\infty}}, \tag{25}$$

where $H = H_0(1 + C_p^2)^{1/2}$.

To prove inequality (22), we assume that u_1 and u_2 satisfy (20) with coefficients $A_1 = e^{q_1} = \eta_1$ and $A_2 = e^{q_2} = \eta_2$. Hence, subtracting the term $\nabla \cdot (e^{q_1} \nabla u_2)$, the difference $u_2 - u_1$ satisfies the equation

$$\nabla \cdot (e^{q_1} \nabla (u_2 - u_1)) = \nabla \cdot ((e^{q_1} - e^{q_2}) \nabla u_2) + e^{q_2}(e^{\beta u_2} - e^{-\beta u_2}) - e^{q_1}(e^{\beta u_1} - e^{-\beta u_1}).$$

Taking the inner product of this equation with $u_2 - u_1$ leads to

$$\begin{aligned} I :&= \left| \int e^{q_1} \nabla (u_2 - u_1) \cdot \nabla (u_2 - u_1) \right| \\ &= \left| \int (e^{q_1} - e^{q_2}) \nabla u_2 \cdot \nabla (u_2 - u_1) + (e^{q_2}(e^{\beta u_2} - e^{-\beta u_2}) - e^{q_1}(e^{\beta u_1} - e^{-\beta u_1}))(u_2 - u_1) \right|, \end{aligned}$$

where the inequalities

$$e^{-\|q_1\|_{L^\infty}}\|\nabla(u_2-u_1)\|_{L^2}^2 \le I \le \left|\int (e^{q_1}-e^{q_2})\nabla u_2\cdot\nabla(u_2-u_1)\right| + \left|\int (e^{q_2}-e^{q_1})(e^{\beta\max(\lambda_1,\lambda_2)}-e^{-\beta\max(\lambda_1,\lambda_2)})(u_2-u_1)\right|$$

hold because of the triangle inequality and the pointwise estimates $\kappa_i \le u_i \le \lambda_i$, $i \in \{1,2\}$, for the solution of the nonlinear Poisson–Boltzmann equation [30], where κ_i and λ_i are constants.

Now we use the Cauchy–Schwarz and Poincaré inequalities to find

$$e^{-\|q_1\|_{L^\infty}}\|\nabla(u_2-u_1)\|_{L^2} \le I \le \|e^{q_1}-e^{q_2}\|_{L^\infty}(\|\nabla u_2\|_{L^2}+C_p|e^{\beta\max(\lambda_1,\lambda_2)}-e^{-\beta\max(\lambda_1,\lambda_2)}|),$$

where C_p is a Poincaré constant. Since $e^{q(x)}$ ($x \in D$) is continuously differentiable, it is Lipschitz continuous by the Weierstrass Theorem. Thus we have

$$\|e^{q_2}-e^{q_1}\|_{L^\infty} \le \|q_1-q_2\|_{L^\infty} e^{\max(\|q_1\|_{L^\infty},\|q_2\|_{L^\infty})}. \tag{26}$$

Using inequalities (24) and (26), we obtain

$$e^{-\|q_1\|_{L^\infty}}\|\nabla(u_2-u_1)\|_{L^2} \le I \le \|q_1-q_2\|_{L^\infty} e^{\max(\|q_1\|_\infty,\|q_2\|_\infty)}\big(e^{2\|q_2\|_\infty}\big(\|\nabla\overline{g}\|_{L^2}+C_p e^{|\beta\lambda_2|} + C_p e^{|\beta\kappa_2|}\big)+C_p|e^{\beta\max(\lambda_1,\lambda_2)}-e^{-\beta\max(\lambda_1,\lambda_2)}|\big),$$

which leads to

$$\begin{aligned}\|\nabla(u_2-u_1)\|_{L^2} &\le \|q_1-q_2\|_{L^\infty} e^{4\max(\|q_1\|_\infty,\|q_2\|_\infty)}\big(\|\nabla\overline{g}\|_{L^2}+C_p e^{|\beta\lambda_2|}+C_p e^{|\beta\kappa_2|}\\ &\quad + C_p|e^{\beta\max(\lambda_1,\lambda_2)}-e^{-\beta\max(\lambda_1,\lambda_2)}|\big)\\ &= S_0\|q_1-q_2\|_{L^\infty} e^{4\max(\|q_1\|_\infty,\|q_2\|_\infty)},\end{aligned}$$

where $S_0 := \|\nabla\overline{g}\|_{L^2}+C_p e^{|\beta\lambda_2|}+C_p e^{|\beta\kappa_2|}+C_p|e^{\beta\max(\lambda_1,\lambda_2)}-e^{-\beta\max(\lambda_1,\lambda_2)}|$. Now, we can write

$$\begin{aligned}\|u_1-u_2\|_{H^1} &\le (1+C_p^2)^{1/2}\|\nabla(u_1-u_2)\|_{L^2}\\ &\le (1+C_p^2)^{1/2}\big(\|\nabla\overline{g}\|_{L^2}+C_p e^{|\beta\lambda_2|}+C_p e^{|\beta\kappa_2|}+C_p|e^{\beta\max(\lambda_1,\lambda_2)}-e^{-\beta\max(\lambda_1,\lambda_2)}|\big)\\ &\quad\times\ e^{4\max(\|q_1\|_\infty,\|q_2\|_\infty)}\|q_1-q_2\|_{L^\infty}\\ &= S e^{4\max(\|q_1\|_\infty,\|q_2\|_\infty)}\|q_1-q_2\|_{L^\infty},\end{aligned}$$

where $S := S_0(1+C_p^2)^{1/2}$, which completes the proof for the nonlinear equation (20). □

Remark 1. The quantity $\|\nabla\overline{g}\|_{L^2(D)}$ is non-zero even if the Dirichlet datum g is a constant. The new variable $v := u-\overline{g}$ is defined such that $\overline{g} = g$ on ∂D and $\overline{g}$ is arbitrary in D. Therefore in the (realistic) case of non-constant g, $\|\nabla\overline{g}\|_{L^2(D)}$ is non-zero in D. Hence, even if $f=0$, the quantities F, H, and S are non-zero.

We summarize the above results for nonlinear elliptic inverse problems in the following theorem:

Theorem 1. *Assume $G(q)=u$ is the observation operator representing the solution u of the real-valued nonlinear equation (20) in the bounded domain $D\subset\mathbb{R}^n$, $n\in\{2,3\}$, with a smooth boundary ∂D and $A=\exp(q)=\eta$ with $q\in L^\infty(D)$. Then the estimates*

$$|G(q)| \le H\exp(2\|q\|_{L^\infty(D)}) \tag{27}$$

and

$$|G(q_1)-G(q_2)| \le S\exp(4\max\{\|q_1\|_{L^\infty(D)},\|q_2\|_{L^\infty(D)}\})\|q_1-q_2\|_{L^\infty(D)} \tag{28}$$

hold, where $H=H(\|\nabla\overline{g}\|_{L^2})$ and $S=S(\|\nabla\overline{g}\|_{L^2})$, which have been defined in Proposition 1.

The estimates (27) and (28) for real and imaginary parts of the solution yield estimates for the complex-valued equation (20) as well. Therefore, Assumption 2 are satisfied for the general EIT model equations (20), where g is

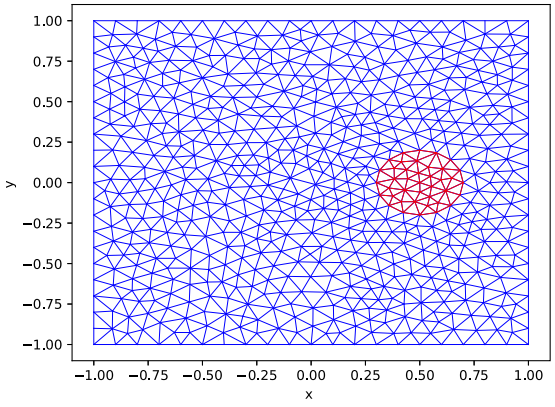

Fig. 2. Simulated EIT domain for the test problem containing a circle-shaped inclusion centered at $(0.5, 0)$ with radius of 0.2.

constant at each contact at the surface of the device. This will lead to the main results of the paper, i.e., well-definedness and well-posedness of the Bayesian inversion problem for linear and nonlinear elliptic problems including the EIT inverse problem.

The posterior probability measure μ^y defined by (16) is well-defined if we show that the measure is normalizable. For well-posedness, the continuity of the posterior measure in the Hellinger metric with respect to the data must be shown. We state the two main theorems resulting from Proposition 1. The reader is referred to [18] for the proofs.

Theorem 2 (*Well-Definedness of the Posterior Measure [18, Theorem 4.1]*)**.** *Let G satisfy Assumption 2 and assume that the prior measure μ_0 is a Gaussian measure satisfying $\mu_0(X) = 1$. Then the posterior measure μ^y given by (16) is a well-defined probability measure.*

The following theorem states the well-posedness for inverse problems by showing Lipschitz continuity of the posterior measure in the Hellinger metric with respect to changes in the data.

Theorem 3 (*Well-Posedness of the Bayesian Inverse Problem [18, Theorem 4.2]*)**.** *Let G satisfy Assumption 2. Assume also that the prior measure μ_0 is a Gaussian measure satisfying $\mu_0(X) = 1$ and that the measure is absolutely continuous, $\mu^y \ll \mu_0$, with its Radon–Nikodym derivative given by (16) for each $y \in Y$.*

Then the posterior measure μ^y is Lipschitz continuous in the data y with respect to the Hellinger distance, i.e., if μ^y and $\mu^{y'}$ are two measures corresponding to data y and y', then there exists $\alpha = \alpha(r) > 0$ such that the inequality

$$d_{\text{Hell}}(\mu^y, \mu^{y'}) \leq \alpha \|y - y'\|_Y$$

holds for all y and y' with $\max\{\|y\|_Y, \|y'\|_Y\} < r$.

4. Bayesian inference for the nonlinear EIT model on a test problem and using synthetic data

In this section, we verify the validity of our presented nonlinear model for the EIT forward problem as well as the proposed inversion method for the backward problem on a test example and using synthetic data. The computational domain here is a square including a circle inhomogeneity with different material from the background medium (see Fig. 2).

To solve the forward model, we have used finite-element method on the prescribed test geometry with 8 electrodes attached to the boundary, which are labeled counterclockwise as electrode 1 to 8, starting from the left bottom. We assume that the background medium is a continuum dielectric and contains an inclusion centered at $(0.5, 0)$ with a different material, whose size, charge and conductivity are quantities of interest in solving the EIT inverse problem here. The choice of the voltage patterns or Dirichlet boundary conditions for the forward problem is important, since it effects the resulting currents and consequently the conservation of current is affected. As it is observable in Table 1, we have chosen the voltage pattern by skipping one contact and applying ± 0.01 V. The results of

Table 1
Four different applied voltage patterns (in volts) in an 8-electrode EIT device configuration. The indices of the voltages are the labels of the electrodes.

Pattern	U_1	U_2	U_3	U_4	U_5	U_6	U_7	U_8
1	0.01	0	−0.01	0	0.01	0	−0.01	0
2	0	0.01	0	−0.01	0	0.01	0	−0.01
3	−0.01	0	0.01	0	−0.01	0	0.01	0
4	0	−0.01	0	0.01	0	−0.01	0	0.01

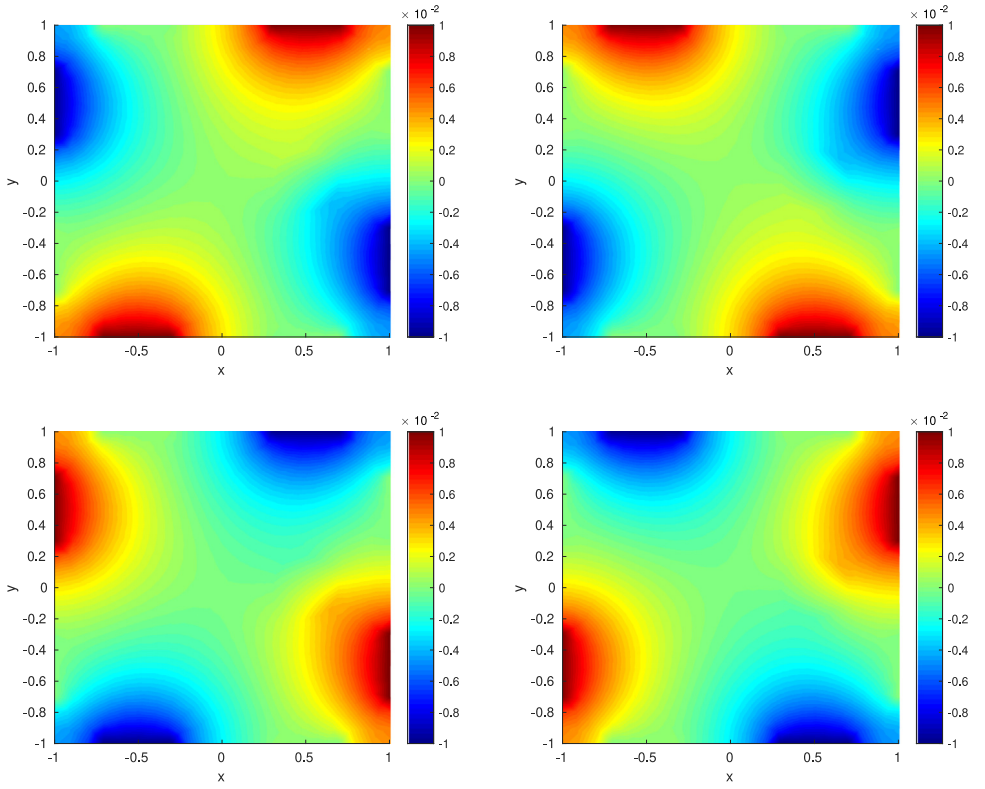

Fig. 3. Electrical potential (in volts) for the 8-electrode EIT device configuration with an inclusion centered at $(0.5, 0)$. The figures illustrate four voltage patterns mentioned in Table 1.

the presented forward EIT model (7) on the prescribed geometry are shown in Fig. 3. This figure illustrates the potential u calculated for four different settings of boundary conditions according to Table 1.

Now everything is ready to solve the nonlinear EIT inverse problem. Our goal is simultaneous extraction of multiple parameters which reflect physical and electrical properties of the interior body in the framework of our theoretical results. To this end, we implement an adaptive MCMC method, namely the delayed-rejection adaptive Metropolis (DRAM) algorithm as a package in the Julia programming language [25,26] to show this inversion algorithm is capable of dealing with the nonlinearity and ill-posedness of our test problem. Here, the electrical currents are calculated on the eight electrodes in four different patterns/boundary conditions in the nonlinear Poisson–Boltzmann equation, which is solved for the parameter values $A = 3$, $R = 0.2$, and $Q = 1$. These values are used as synthetic data in the Bayesian inversion process.

Fig. 4 displays the marginal histograms of the posterior distributions of the parameters A, Q and R as the quantities of interest in the EIT problem at hand. This figure illustrates a very good reconstruction results in the EIT test problem. It is an advantage of the statistical method of Bayesian inference that it gives confidence interval containing admissible and optimal values for each unknown quantity if we could reconstruct it.

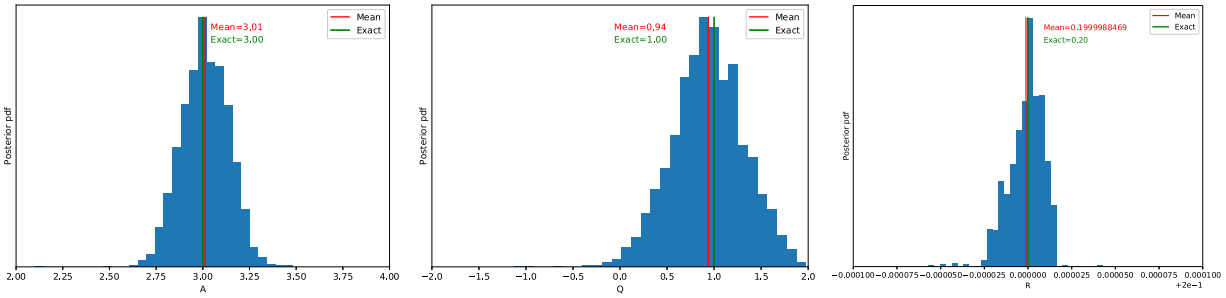

Fig. 4. Marginal histograms of posterior distributions of the parameters A, Q and R produced by means of the DRAM algorithm using 10 000 samples. The mean of the produced chain and the exact value of the parameters are indicated on the figures.

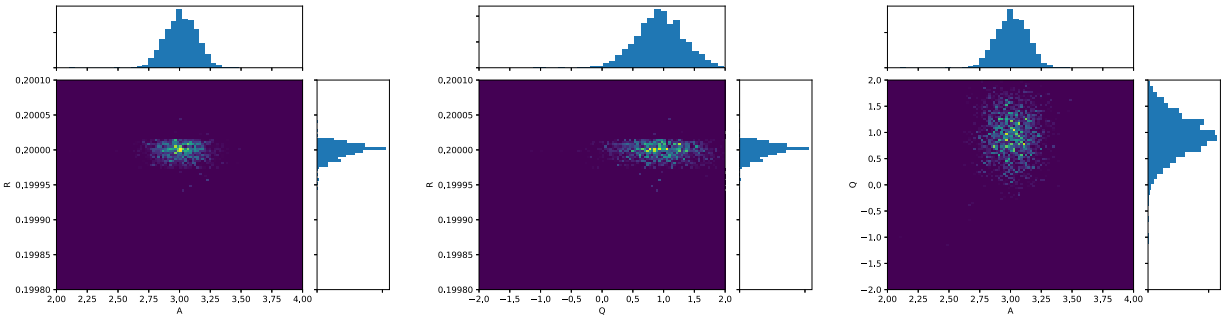

Fig. 5. Two-dimensional histograms and marginal posterior distributions for the 8-electrode EIT device configuration and for 10 000 samples obtained by the DRAM algorithm for the parameters A, Q and R. The figures show correlations between each pair of the parameters.

The estimated mean value of the generated posterior chains for the parameter A, R and Q are 3.01, 0.1999988 and 0.94, respectively. Having computed the mean and standard deviation of the chains, we can calculate the interval of admissible values of the parameters with 95% of confidence. According to Bayesian estimation results, this interval for parameters A, Q and R respectively are $A \in [2.76, 3.26]$, $R \in [0.199979, 0.200019]$, and $Q \in [0.18, 1.69]$, which shows a successful reconstruction for each of the EIT unknown quantities in the test problem. Here, the above mentioned confidence intervals and inferred values are obtained using the complete Markov-chain of size 10 000. However, if we use for example the last 1000 samples as the effective posterior samples, the results are even better; the confidence intervals of $A \in [2.80, 3.22]$, $R \in [0.199984, 0.200018]$ and $Q \in [0.30, 1.66]$ are obtained and the inferred values are also much closer to the exact ones: 3.01, 0.2 and 0.98 as mean values of the unknown parameters A, R and Q, respectively.

Fig. 5 illustrates correlation between each pair of the parameters and their marginal posterior distributions. Bayesian inference results show that the size of the inclusion can be extracted very accurately. Conductivity and charge (and charge sign) of the inclusion are the other parameters of interest that can be recovered nicely using Bayesian inversion. The whole computational method including the forward model solver and the MCMC calculations is computationally expensive since the physical model must be evaluated for thousands of samples iteratively. The intensive work is spent on the generation of the mesh due to the fact that the size of the inclusion is one of the quantities of interest and therefore the process of mesh generation must be iterated for each sample.

To statistically test the correlation between the samples of generated Markov chains, we look at the autocorrelation function (ACF). Fig. 6 displays autocorrelation plots for the three Markov chains associated with the three parameters. The results illustrate independence of samples and good mixing in the generated chains.

5. Bayesian inference for the nonlinear EIT model on a cross-section of leg and using measurement data

In the previous section, we tested the new EIT model and the proposed inversion method on a square domain with an inclusion using synthetic data and extracted the model unknown parameters, successfully. In this section,

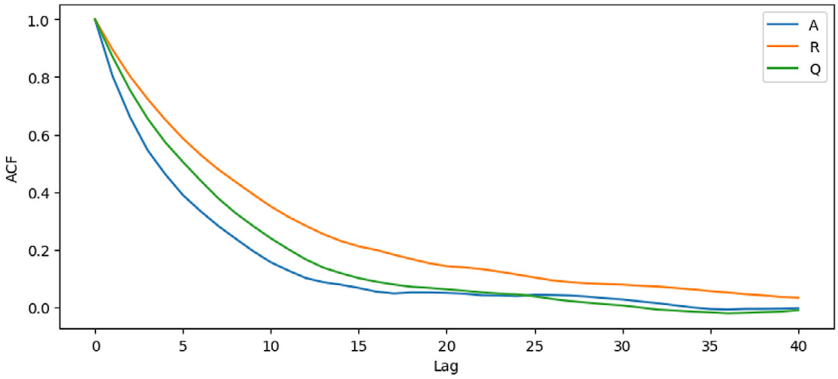

Fig. 6. Autocorrelation plots of the generated Markov chains by the DRAM algorithm for the three parameters of interest.

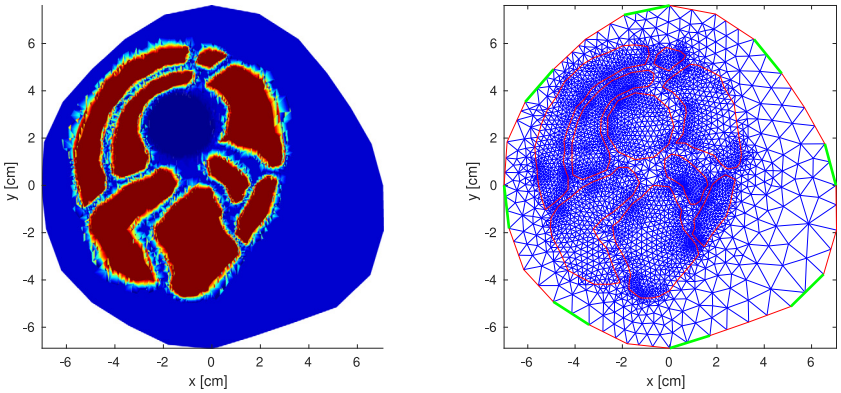

Fig. 7. EIT domain: cross-section of a right leg illustrating a schematic of the three subdomains (left) and the discretization by a FEM mesh (right) used for solving the forward problem.

our aim is to establish the new nonlinear model by applying the methodology on a real-world problem, namely the extraction of muscle conductivity in a cross-section of a human right leg using measurement data. As we already mentioned, the presented model is able to distinguish liquids due to the nonlinear term, and therefore the electrical properties of a muscle in the body can be estimated more precisely, which leads to design of reliable EIT sensors and the reconstruction of higher resolution images. First, we describe the computational domain and illustrate the numerical solution of the proposed EIT model on the domain. Then we explain the measurement data collection and present the numerical results of the inversion method.

5.1. The computational domain and the solution of the forward problem

The computational domain is a cross-section of a human right leg, where eight electrodes are attached to its boundary. Fig. 7 (right) shows the domain with finite element discretization. In this figure (left), three different subdomains are displayed: the first subdomain is a circle bone (in dark blue) surrounded by the second subdomain muscle (in brown), which itself consists of many partitions, and the rest is fat (in blue). Each subdomain has its own electrical conductivity and in the solution of the forward problem the FEM mesh is aligned with the inclusions such that each element has a constant value for the coefficient A.

To solve the nonlinear forward problem, we have used the first order Galerkin finite element method on the three subdomains. In this geometry, eight electrodes are attached to the boundary, which are labeled clockwise as electrode 1 to 8, starting from the top. In the simulations, we assume that voltages of ± 10 V are applied to the

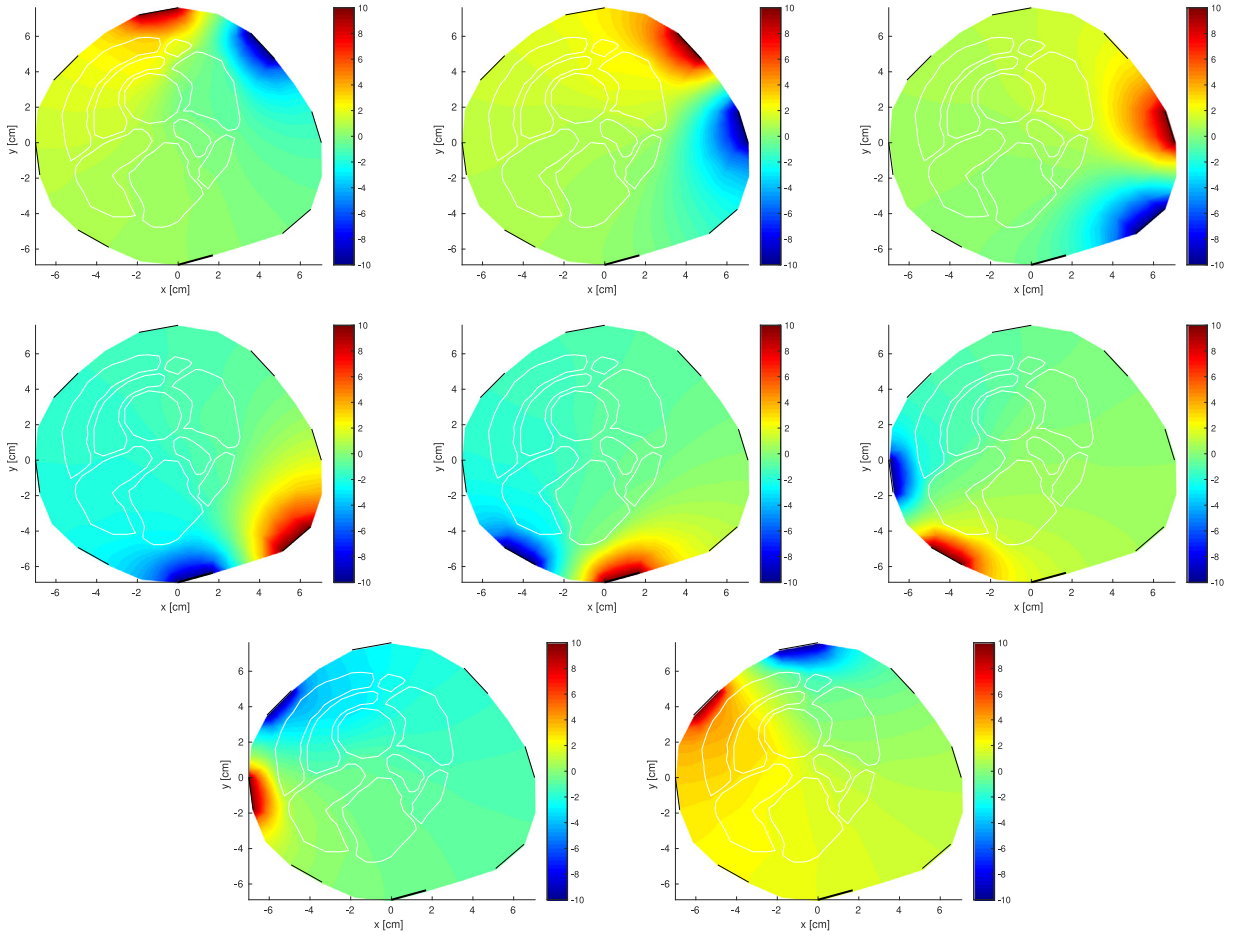

Fig. 8. Solution of the nonlinear forward problem (in volts) using neighboring injection method for a cross-section of a right leg.

injection electrode pairs under the neighboring/adjacent method. Fig. 8 displays the obtained electrical potential as the solution of the model on the cross-section of the right leg using eight injection patterns.

5.2. Measurement data collection and solution of the inverse problem

Here, we aim to solve the EIT inverse problem corresponding to the nonlinear model that we solved in Section 5.1 on the cross-section of a right leg using real-world surface electrode measurements. The goal is to identify the electrical conductivity of muscle tissue inside the leg. To solve this ill-posed and nonlinear inverse problem and reconstruct the conductivity of muscle tissue, we propose the Bayesian techniques, and in particular an adaptive MCMC method, namely the DRAM algorithm, which has already proved its capability for solving such sophisticated inverse problems on an EIT test problem in Section 4. For Bayesian analysis of this real-world example, we use measured data and the neighboring injection method. The reported interval for the muscle conductivity by Gabriel [39] is $[0.02, 0.6]$ S/m. The reconstruction result shows an acceptable interval of $[0.03, 0.10]$ S/m for the parameter value with 95% of confidence and the mean value of 0.07 S/m (see Fig. 9).

To interpret the results generated by the Bayesian estimation method, we look at how independent the produced samples are and how good the mixing of the chains is. To this end, we calculate the autocorrelation between the samples of the posterior chain [40]. Fig. 10 illustrates autocorrelation plot of the estimated posterior Markov-chain using all the measurement data, which is indicated as the main chain. This figure also shows ACF plots for each of injection patterns.

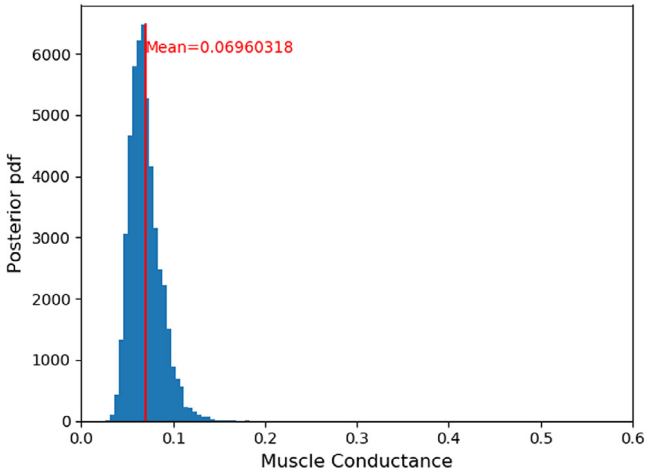

Fig. 9. Posterior distribution of the reconstructed conductivity of muscle using the nonlinear forward model for the cross-section of a right leg.

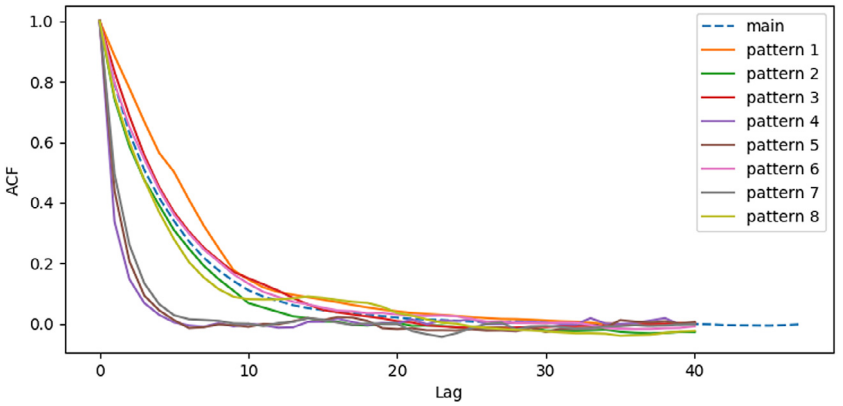

Fig. 10. Autocorrelation plots of the posterior chains of eight experimental patterns and the main posterior chain using all the measurement patterns simultaneously.

6. Conclusions

In this work, we presented a comprehensive physical model for electrical-impedance tomography sensors with applications in medicine and healthcare. The developed EIT model has the advantage of distinguishing between liquids and tissues in the body, which is crucial to design a reliable EIT sensor for high resolution images. In EIT applications, for instance in medicine, there are big data sets of measurements which need to be statistically analyzed to infer the electrical properties in order to help diagnosis and treatment. To this end, we proposed Bayesian inversion methods and formulated the methodology for the new governing model in a measure-theoretic framework and in an infinite-dimensional setting and then proved well-definedness of the posterior measure and well-posedness of the Bayesian inversion for the presented nonlinear model. We checked the validity of the new model and the proposed inverse method first on a simple domain including an inhomogeneity with different electrical properties from the background medium and using synthetic data in order to reconstruct conductivity, charge and size of the inhomogeneity. Then we established the methodology by applying it on a real-world application in medicine using measurement data to reconstruct the electrical conductivity of muscle tissue in a cross-section of a human leg. The numerical results illustrate a reliable reconstruction due to the established reported database for the admissible electrical conductivity of tissues.

Acknowledgment

This work was supported by FWF (Austrian Science Fund) START project Y660 *PDE Models for Nanotechnology*.

References

[1] D.S. Holder, Electrical Impedance Tomography: Methods, History and Applications, CRC Press, 2004.
[2] S.J. Stanley, G.T. Bolton, A review of recent electrical resistance tomography (ERT) applications for wet particulate processing, Part. Part. Syst. Charact. 25 (3) (2008) 207–215.
[3] M. Soleimani, W.R. Lionheart, Nonlinear image reconstruction for electrical capacitance tomography using experimental data, Meas. Sci. Technol. 16 (10) (2005) 1987.
[4] M. Cheney, D. Isaacson, J.C. Newell, Electrical impedance tomography, SIAM Rev. 41 (1) (1999) 85–101.
[5] A.L. Ramirez, W.D. Daily, A.M. Binley, Electrical Resistance Tomography, Tech. Rep., Pacific Northwest National Lab., Richland, WA (US), 2000.
[6] W.R. Gilks, S. Richardson, D. Spiegelhalter, Markov Chain Monte Carlo in Practice, Chapman & Hall, 1996.
[7] C.P. Robert, G. Cassella, Monte Carlo Statistical Methods, Springer Verlag, 1999.
[8] M. Sambridge, K. Mosegaard, Monte Carlo methods in geophysical inverse problems, Rev. Geophys. 40 (3) (2002) 1–29.
[9] K. Mosegaard, M. Sambridge, Monte Carlo analysis of inverse problems, Inverse Problems 18 (3) (2002) R29.
[10] J.S. Rosenthal, et al., Optimal proposal distributions and adaptive MCMC, in: Handbook of Markov Chain Monte Carlo, Vol. 4, CRC Press, Boca Raton, FL, 2011.
[11] H. Haario, M. Laine, A. Mira, E. Saksman, DRAM: efficient adaptive MCMC, Stat. Comput. 16 (4) (2006) 339–354.
[12] S.L. Cotter, G.O. Roberts, A.M. Stuart, D. White, MCMC methods for functions: modifying old algorithms to make them faster, Statist. Sci. (2013) 424–446.
[13] A. Nissinen, L. Heikkinen, J. Kaipio, The Bayesian approximation error approach for electrical impedance tomography–experimental results, Meas. Sci. Technol. 19 (1) (2008).
[14] J.P. Kaipio, V. Kolehmainen, E. Somersalo, M. Vauhkonen, Statistical inversion and Monte Carlo sampling methods in electrical impedance tomography, Inverse Problems 16 (5) (2000) 1487.
[15] L. Roininen, J.M. Huttunen, S. Lasanen, Whittle–Matérn priors for Bayesian statistical inversion with applications in electrical impedance tomography, Inverse Probl. Imaging 8 (2) (2014) 561–586.
[16] M.M. Dunlop, A.M. Stuart, The Bayesian formulation of EIT: Analysis and algorithms, Inverse Probl. Imaging 10 (4) (2016) 1007–1036.
[17] M. Lassas, E. Saksman, S. Siltanen, Discretization-invariant Bayesian inversion and Besov space priors, Inverse Probl. Imaging 3 (1) (2009) 87–122.
[18] A.M. Stuart, Inverse problems: a Bayesian perspective, Acta Numer. 19 (2010) 451–559.
[19] M. Dashti, A.M. Stuart, The Bayesian approach to inverse problems, in: Handbook of Uncertainty Quantification, Springer, 2016, pp. 1–118.
[20] C. Geuzaine, J.-F. Remacle, Gmsh: A 3-D finite element mesh generator with built-in pre-and post-processing facilities, Internat. J. Numer. Methods Engrg. 79 (11) (2009) 1309–1331.
[21] H. Haario, E. Saksman, J. Tamminen, Adaptive proposal distribution for random walk Metropolis algorithm, Comput. Stat. 14 (3) (1999) 375–396.
[22] H. Haario, E. Saksman, J. Tamminen, et al., An adaptive Metropolis algorithm, Bernoulli 7 (2) (2001) 223–242.
[23] L. Tierney, A. Mira, Some adaptive Monte Carlo methods for Bayesian inference, Stat. Med. 18 (1718) (1999) 2507–2515.
[24] P.J. Green, A. Mira, Delayed rejection in reversible jump Metropolis–Hastings, Biometrika 88 (4) (2001) 1035–1053.
[25] J. Bezanson, A. Edelman, S. Karpinski, V.B. Shah, Julia: A fresh approach to numerical computing, SIAM Rev. 59 (1) (2017) 65–98.
[26] J. Bezanson, et al., Julia: the Julia programming language, 2018, https://julialang.org/.
[27] O. Scherzer, Handbook of Mathematical Methods in Imaging, Springer Science & Business Media, 2010.
[28] J. Kaipio, E. Somersalo, Statistical and Computational Inverse Problems, Vol. 160, Springer Science & Business Media, 2006.
[29] A. Adler, W.R. Lionheart, Uses and abuses of EIDORS: an extensible software base for EIT, Physiol. Meas. 27 (5) (2006) S25.
[30] S. Baumgartner, C. Heitzinger, Existence and local uniqueness for 3D self-consistent multiscale models for field-effect sensors, Commun. Math. Sci. 10 (2) (2012) 693–716.
[31] R.C. Smith, Uncertainty Quantification: Theory, Implementation, and Applications, Vol. 12, SIAM, 2013.
[32] A. Gelman, J.B. Carlin, H.S. Stern, D.B. Dunson, A. Vehtari, D.B. Rubin, Bayesian Data Analysis, CRC Press, 2013.
[33] A. Tarantola, Inverse Problem Theory: Methods for Data Fitting and Model Parameter Estimation, Elsevier, New York, 1987.
[34] W.P. Gouveia, J.A. Scales, Resolution of seismic waveform inversion: Bayes versus Occam, Inverse Problems 13 (2) (1997) 323–349.
[35] B. Stadlbauer, A. Cossettini, D. Pasterk, P. Scarbolo, L. Taghizadeh, C. Heitzinger, L. Selmi, et al., Bayesian estimation of physical and geometrical parameters for nanocapacitor array biosensors, J. Comput. Phys. 397 (2019) 108874.
[36] L. Taghizadeh, A. Karimi, E. Presterl, C. Heitzinger, Bayesian inversion for a biofilm model including quorum sensing, Comput. Biol. Med. 117 (2020) 103582.
[37] E.K. Lenzi, L.R. Evangelista, L. Taghizadeh, D. Pasterk, R.S. Zola, T. Sandev, C. Heitzinger, I. Petreska, Reliability of Poisson–Nernst–Planck anomalous models for impedance spectroscopy, J. Phys. Chem. B 123 (37) (2019) 7885–7892.
[38] M. Dashti, A.M. Stuart, Uncertainty quantification and weak approximation of an elliptic inverse problem, SIAM J. Numer. Anal. 49 (6) (2011) 2524–2542.
[39] C. Gabriel, Compilation of the Dielectric Properties of Body Tissues at RF And Microwave Frequencies, Tech. Rep., King's Coll London (United Kingdom) Dept of Physics, 1996.
[40] G.E. Box, G.M. Jenkins, G.C. Reinsel, G.M. Ljung, Time Series Analysis: Forecasting and Control, John Wiley & Sons, 2015.